

Structure, dielectric and optical properties of transparent Nd³⁺: KNbO₃ nanocrystalline glass-ceramics

Reenamoni Saikia Chaliha ^a, K. Annapurna ^a, Anal Tarafder ^a,
V. S. Tiwari ^b, P. K. Gupta ^b and Basudeb Karmakar ^{a,*}

^a *Glass Science and Technology Section, Central Glass and Ceramic Research Institute
(Council of Scientific and Industrial Research)
196, Raja S.C. Mullick Road, Kolkata 700032, India*

^b *Laser Materials Development and Devices Division, Raja Ramanna Center for
Advanced Technology, Indore 452 013, India*

Abstract

Here, glass in the composition of 25K₂O-25Nb₂O₅-50SiO₂ (mol %) doped with Nd₂O₃ (0.5 wt% in excess) was isothermally crystallized at 800°C for 1-100 h. Their structures, dielectric and optical properties were analyzed with the progress of nanocrystallization of Nd³⁺: KNbO₃ by XRD, FESEM, TEM, FTIRRS, DC, optical absorption and fluorescence measurements. Crystallization of KNbO₃ is confirmed from XRD and the appearance of 749 cm⁻¹ band in the FTIRRS spectra. The crystallite size estimated from XRD and TEM is found to vary in the range 7-11 nm. The formation of ferroelectric nano-crystalline KNbO₃ phase is also attributed by a steep rise in the dielectric constant (ε) of glass-ceramics with heat-treatment time. The measured photoluminescence spectra have exhibited emission transitions of ⁴F_{3/2} → ⁴I_J (J = 9/2, 11/2 and 13/2) from Nd³⁺ ions upon excitation at 817 nm. It is observed that the photoluminescent intensity and excited state lifetime of Nd³⁺ ions initially decrease and then gradually increase with increase in heat-treatment time. The absorption spectra and

fluorescence measurements disclose that the Nd^{3+} ions gradually enter into the KNbO_3 nanocrystals.

Keywords: Transparent glass-ceramic, Nano-crystallized Nd^{3+} : KNbO_3 , Luminescence, Ferroelectric crystals, Dielectric constant.

*Corresponding author. Tel.: +91-33 2473 3469; fax: +91-33 2473 0957

E-mail address: basudebk@cgcricri.res.in (B. Karmakar)

1. Introduction

Potassium niobate (KNbO_3 , KN) is a well known ferroelectric material with the $\text{A}^{1+}\text{B}^{5+}\text{O}_3$ perovskite-type (orthorhombic) crystal structure with crystal symmetry class $mm2$ (unit cell dimensions : $a = 5.6896 \text{ \AA}$, $b = 3.9693 \text{ \AA}$ and $c = 5.7256 \text{ \AA}$) and having large nonlinear coefficient ($d_{33} = 27.4 \text{ pm/V}$ at 1064 nm) [1]. Due to its applications in photonic and optoelectronic devices such as frequency doubling, tunable wave guiding, active laser host, holographic storage and surface acoustic wave, KNbO_3 becomes a subject of intense study [2, 3]. Very recently, potassium niobate ceramics were revisited in the interest of a search for environmental friendly lead-free piezoelectric and nonlinear materials [4]. In addition to those, there has been an increasing academic and technological interest in crystallized glasses containing KNbO_3 ferroelectric as an active crystalline phase because of its low cost and high speed fabrication process of glass technology, compared to single crystal preparation, accompanied by the flexibility of tailored properties to produce transparent nanostructures by controlled crystallization. A large electro-optic effect ($r_{42} = 380 \text{ pm/V}$ for KNbO_3 [1]) has been observed in a number of transparent glass-ceramic materials containing a ferroelectric crystalline phase. Several isothermal or non-isothermal studies have been carried out with a view to generate KNbO_3 , KNbSi_2O_7 , $\text{K}_3\text{Nb}_3\text{Si}_2\text{O}_{13}$ etc. ferroelectric crystal phases in various compositions of the $\text{K}_2\text{O-Nb}_2\text{O}_5\text{-SiO}_2$ (KNS) glass system [5-10] and noticed strong second harmonic generation (SHG). It is anticipated that, when doped with rare earth (RE) ions, these glass-ceramics become very good luminescent media which are able to generate and amplify light. This ability, combined with inherent nonlinear optical (NLO) properties of ferroelectric crystals, could offer a possibility to design self frequency doubling laser

sources [1]. Therefore, it is considered more interesting and important to explore crystallization of RE doped glasses. To the best of our knowledge, studies on nanostructured crystallization of neodymium (III), Nd^{3+} ion doped $\text{K}_2\text{O-Nb}_2\text{O}_5\text{-SiO}_2$ glasses have not been reported previously.

Among the rare earths, Nd^{3+} has been extensively used as laser active ion in several hosts due to high quantum efficiency of its some of the emission channels either by normal fluorescence in NIR region or by upconversion/frequency doubling in green – red wavelengths [11-13]. Most of the Nd^{3+} lasers operate in NIR region on two lasing transitions ${}^4\text{F}_{3/2} \rightarrow {}^4\text{I}_{11/2, 13/2}$ at around 1060 nm and 1349 nm wavelengths respectively based on four level systems. However, the emission around 900 nm due to transition ${}^4\text{F}_{3/2} \rightarrow {}^4\text{I}_{9/2}$ in Nd^{3+} doped materials has not been explored much for the lasing action because of the fact that this quasi-three level system may suffer from re-absorption losses. But under suitable conditions, laser operation at this wavelength may be possible [14]. Moreover, the emission in the blue wavelength may be realized by frequency doubling phenomenon if the emission from transition ${}^4\text{F}_{3/2} \rightarrow {}^4\text{I}_{9/2}$ could be efficient. Apart from its high quantum efficiency performance as laser active ion, Nd^{3+} has also been well exploited as a structural probe in studying the local field effects around the dopant ions [15] as it possesses hypersensitive transitions.

The dielectric behavior of amorphous solids (here glass) differs widely from that of crystalline solids (here glass-ceramics). This difference is remarkably large in the cases of ferroelectric crystals due to their high spontaneous polarization ($P_s = 0.41 \text{ C/m}^2$ for KNbO_3) as well as induced polarization under applied electric field [1]. Hence, a

study has also been undertaken on the dielectric properties (dielectric constant) with progress of crystallization of precursor glasses of ferroelectric crystals.

Keeping in view of the significant and potential advantages as stated above, in the present study we focus our systematic analysis on structure, luminescence and dielectric properties of isothermally nanostructured crystallization of Nd^{3+} -doped (0.5 wt% Nd_2O_3 in excess) $25\text{K}_2\text{O}-25\text{Nb}_2\text{O}_5-50\text{SiO}_2$ (mol%) glasses. Here, we have examined the NIR emission of Nd^{3+} doped KNbO_3 crystalline glass-ceramics and its preformed glass as a function of heat treatment duration. Also the bulk glass crystallization process has been studied by differential thermal analysis (DTA), X-ray diffraction (XRD), field emission scanning electron microscopy (FESEM), transmission electron microscopy (TEM) and Fourier transform infrared reflection spectroscopy (FTIRRS).

2. Experimental

The glass in the chemical composition of $25\text{K}_2\text{O}-25\text{Nb}_2\text{O}_5-50\text{SiO}_2$ (mol %) doped with 0.5 wt% Nd_2O_3 (in excess) was prepared using high purity K_2CO_3 (GR, 99%, Alfa Aesar), Nb_2O_5 (GR, 99.5%, Alfa Aesar), SiO_2 (99.99%) and Nd_2O_3 (99.99%, Alfa Aesar) by melting the well mixed chemical batch of 100 g glass in a platinum crucible at 1550°C for 2 h. The melt was homogenized with intermittent stirrings and later it was quenched by pouring the melt onto a pre-heated iron mould. In order to remove the internal stresses the glass block was subsequently annealed at 600°C for 1 h. The as-prepared glass block was cut into desired dimensions and polished for undertaking different measurements.

The density of as-prepared glass was measured by following the standard Archimedes' principle using water as the buoyancy liquid. The refractive indices (n_F , n_e ,

n_C) of glass at three different wavelengths ($\lambda_F = 480.0$ nm, $\lambda_e = 546.1$ nm and $\lambda_C = 643.8$ nm) were measured by a Pulfrich refractometer (Model PR2). The DTA curve of powdered glass was recorded on a Netzsch STA 409 C/CD instrument from the room temperature to 1000°C at a heating rate of 10°C/min. The polished samples were subjected to two steps heat-treatment with initial nucleation at 720°C temperature for 2 h followed by crystallization at 800°C for 1, 2, 3, 5, 10, 25, 50 and 100 h. The resulted glass and glass-ceramic samples were labeled as A, B, C, D, E, F, G, H and I respectively for convenience.

The XRD pattern was recorded using an Xpert-Pro diffractometer (CuK α) with nickel filtered and anchor scan parameters wavelength of 1.54060 Å at 25°C having the source power of 40 kV and 30 mA to identify the possible phases. The nanocrystallinity of the heat-treated glasses was examined by both FESEM and TEM. A Carl Zeiss high resolution Field Emission Electron Microscope (FESEM), model SUPRA 35 VP detector (lithium doped silicon) with the parameters gun vacuum = 3×10^{-10} mbar, system vacuum = 2.65×10^{-5} mbar and extractor current = 159.3 μ A was used for FESEM measurement. Freshly fractured surfaces of the heat-treated glasses were etched in 1% HF solution for 90 s and were coated with a thin carbon film for the above measurements. And the TEM was done on FEI (Tecnai G²) instrument. The dielectric constant of all samples was measured at room temperature using a Hioki LCR meter (Model 3532-50 Hitester) at 1 MHz frequency after coating with a conductive silver paint followed by drying at 140°C for 1h.

The FTIR reflectance spectra of all Nd³⁺-doped glass and glass-ceramics were recorded using a Perkin Elmer FTIR spectrometer (Model 1615) in the wavenumber

range 400-2000 cm^{-1} with a spectral resolution of $\pm 2 \text{ cm}^{-1}$ and at a 15° angle of incidence. The fluorescence emission and excitation spectra of the Nd^{3+} doped as-prepared and heat-treated samples were measured on an enhanced performance NIR continuous bench top modular spectrofluorometer of Photon Technology International (PTI) attached with Hamamatsu NIR-PMT (P1.7R) as detector and Xe arc lamp as excitation source. The lifetime was measured with the same instrument using Xe flash lamp of 60 W.

3. Results and discussion

3.1 Physical, optical and thermal properties

The prepared glass was transparent. From the measured glass density and refractive indices (n_e , n_F' and n_C') at three different wavelengths, other related optical properties have been determined using relevant expressions and the results are presented in Table 1. From Table 1 it is clear that the refractive index and density of potassium niobium silicate glass are higher than those of normal soda lime silicate glasses (RI = 1.5). The large refractive indices of these glasses are due to the presence of highly polarizable Nb^{5+} ions with high ionic refraction ($R_i = 24.5$) [16]. It is observed that ions with an empty or unfilled d-orbital such as Nb^{5+} ion (outer electronic configuration: $4d^05s^0$) contributes very strongly to the linear and nonlinear polarizabilities [17]. For the same reason, this glass possesses a high value of molar refractivity ($R_M = 15.86 \text{ cm}^3$) and electronic polarizability ($\alpha = 6.286 \times 10^{-24} \text{ cm}^3$) [18, 19].

The DTA curve recorded for the as-prepared powdered glass sample is shown in Fig. 1, which exhibited an inflection in the temperature range 642-677°C followed by two

exothermic peaks at 760°C (T_{p1}) and 935°C (T_{p2}) corresponding to the phase crystallization. The point of intersection of the tangents drawn at the slope change marked in Fig. 1 of the DTA curve estimates the glass transition temperature (T_g). These are listed in Table I. From the DTA data, the glass thermal stability factor ($\Delta T = T_{p1} - T_g$) has been determined and found to be 91°C. Reasonably, high glass stability factor specifies the ability of this glass in forming nano-structured glass-ceramic under controlled heat-treatment. The first exothermal peak in the DTA thermogram can be attributed to the growth of KNbO_3 crystallites from nuclei in the glass bulk. The heat-treated glass-ceramics were also transparent as the precursor glass. The transparencies of the glass and resultant nano glass-ceramics are shown in Fig. 2 as they are laid down on writing.

3.2 XRD analysis

Fig. 3(a) shows the X-ray diffraction patterns of as-prepared glass along with the glass-ceramic samples. The amorphous nature of the as-prepared glass is indicated by the XRD pattern consisting of only a broad and halo band at around 29° diffraction angle. The structuring of this halo band takes place in the XRD pattern of the heat-treated glass-ceramic samples (B-I) along with the appearance of other well defined peaks at around 25°, 28.5°, 30°, 32.8° and 51.5° diffraction angles, which confirms the precipitation of crystalline phase in the amorphous matrix. The crystalline phase resembles the JCPDS file cards 32-821 and 32-822 of known potassium niobate. Using the following Scherrer's formula, the average crystallite sizes (diameter, d) were calculated from the full width at

half maximum (FWHM) values of the diffraction peaks detectable in the traces B-I of Fig. 3(a) [20]

$$d = 0.9\lambda/\beta \cos\theta \quad (1)$$

where λ is the wavelength of X-ray radiation ($\text{CuK}\alpha = 1.5406\text{\AA}$), β is the full width at half maximum (FWHM) of the peak at 2θ . The diffraction peak located at $2\theta = 30^\circ$ has been considered for this estimation. The calculated average crystallite sizes lie in the range 7-11 nm. The gradual increase of crystallite size as a function of heat-treatment duration is presented in Fig. 3(b).

3.3 FESEM and TEM image analyses

The morphology and crystallite size in glass-ceramic samples have been examined by FESEM and TEM image analyses. The FESEM photomicrographs of the sample heat-treated at 800°C for 5 and 100 h duration are presented in Figs. 4(a) and 4(b) respectively. From the FESEM micrographs, it is clearly observed that the glassy matrix of the heat-treated samples initially phase separated on nanometric scale followed by incipient precipitation of defined crystallites within the Nb-K rich phase regions on the prolonged heat-treatments. The droplets have irregular shape spreading out uniformly through out the bulk glass matrix and the size of which can be estimated to be about 58-77 nm. The TEM and high resolution TEM (HRTEM) images of the sample heat treated for 100 h have also been presented in Figs 4(c) and 4(d) respectively. The inset in Fig. 4(c) represents its selected area electron diffraction (SAED) image. The atomic or lattice fringes of formed crystallites have been clearly observed in HRTEM image and the distance between any two planes is found to be 4.8 \AA . The formed lattice planes from the

HRTEM image resemble the plane in the JCPDS card file 32-822 of known potassium niobate. Another interesting result is arising out of the comparison of the FESEM and TEM micrographs with the XRD data. The size of the crystallites (7-11 nm) estimated from the XRD patterns and TEM are lesser than the one of the droplets observed in FESEM (58-77 nm), suggesting that the crystallization starts at the interface between the droplets and the matrix. The growth of the crystallites takes place inside these droplets and the droplets are polycrystalline. This phenomenon causes a change of the matrix composition, which prevents the further growth of the crystallites, regardless of the increase in the heat-treatment time, and a stable transparent biphasic structure by a change of the density of inhomogeneities in the matrix is formed [9, 21].

3.4 Fourier transform infrared reflectance spectroscopy

Fig. 5 shows the comparative FTIR reflectance (FTIRRS) spectra of the as-prepared glass (A) and samples heat-treated at 800°C for 1 (B) and 100 h (I) duration in the wavenumber range 400-2000 cm^{-1} and its inset shows the FTIRRS of all the samples in the wavenumber range 400-1500 cm^{-1} . It is seen that the FTIRR spectrum of the as-prepared glass (curve-A) exhibits a broad reflection band centered at 930 cm^{-1} as a result of wider distribution of SiO_4 structural units. This is an indication of the structural disorder exists in the amorphous network with the presence of SiO_4 tetrahedra and NbO_6 octahedra with different number of non-bridging oxygens, and attributed to overlapping of Si-O and Nb-O stretching vibrations. In spite of the transparent nature of the heat-treated samples of 1 and 100 h, their FTIR reflectance spectra (curves B-I) reveal

narrowing of the main reflection band with additional features arising at 1125, 749 and 500-600 cm^{-1} in comparison to the as-prepared glass [6].

Considering the force constant of the Si-O bonds is stronger than that of Nb-O ones, the reflection bands can be assigned in the FTIR reflectance spectra [22]. In the FTIR spectra, the stretching modes of the Si-O-Si bonds of the SiO_4 tetrahedra with nonbridging oxygen (NBO) atoms are active in 900-1000 cm^{-1} range and the stretching modes of the Nb-O bonds in the NbO_6 octahedra occur in the 700-800 cm^{-1} range. It is known that in alkali niobium silicate glasses, NbO_6 octahedra with Nb-O bonds present as a lattice former of KNbO_3 in the Si-O bonds containing SiO_4 tetrahedral network. The alkali ions (here K^+) play the role of charge compensators of excess negative charge at Nb^{5+} cations [23].

It is seen that there are structural modifications occurring in the glass matrix as a result of the heat-treatment as revealed by the variation of the FTIR spectra of the as-prepared glass from that of the heat-treated glasses. It indicates that the heat-treatment changes the composition of the glassy matrix by forming two phases: the one, in the higher wavenumber side enriched of SiO_4 tetrahedra with n bridging oxygen atoms; the other, in the lower wavenumber side mainly containing less-distorted NbO_6 octahedra with no nonbridging oxygens. The latter phase contains a higher amount of K^+ ions as NbO_6 octahedra are negatively charged in order to maintain neutral charge condition. Hence, the rearrangement of the glassy matrix is an indicative of the fact that the alkali enriched phase begins to crystallize producing a nanostructure with the heat-treatment. The reflection bands around 1050-1150 cm^{-1} are associated with the ν_3 antisymmetric stretching vibration modes of the SiO_4 tetrahedra. The symmetric stretching mode ν_1 is

assigned for the reflection bands lying in the range 800-1000 cm^{-1} wavenumber. The reflection band at 1125 and 930 cm^{-1} wavenumber can be related to the asymmetric and symmetric stretching vibration modes of Si-O bonds in SiO_4 tetrahedra respectively, while the band at 749 cm^{-1} is due to the Nb-O stretching modes of distorted NbO_6 octahedra [24, 25]. Hence, it is revealed that in a phase separated matrix of the heat-treated samples, the crystallization starts at the interface between the two phases originating a redistribution of both types of structural units such as NbO_6 octahedra and SiO_4 tetrahedra. This corroborates that the reflection band centered at 749 cm^{-1} wavenumber is assigned as KNbO_3 crystal formation. Very slow increase in the intensity of this reflection band with the increase of heat-treatment time indicates that the further growth of KNbO_3 nanocrystallites at the interface is prevented for longer heat-treatment times to satisfy the chemical composition required by the crystallizing phase [22] but the reflectivity of the 100 h heat-treated sample is very intense than sample heat-treated for 1 h. This is also confirmed by the relative intensity ratio ($I_{\text{Nb-O}}/I_{\text{Si-O}}$) of the reflection bands at 749 to 930 cm^{-1} as given Table 2. Further, all the samples exhibit a band around 598 cm^{-1} in the FTIR spectra as shown in Fig. 5, which is assigned as ν_2 bending vibrational modes of Si-O bonds in the SiO_4 tetrahedra. Thus from the investigations carried out on the measured FTIR reflectance spectra Nd^{3+} doped potassium niobium silicate glass and glass-ceramics as described above provide the information of crystallization with initial phase separation followed by advancement of KNbO_3 crystal formation in the glass matrix. The results of the FTIRRS are in good agreement with that of XRD, FESEM and TEM studies.

3.5 Dielectric constant

As prepared Nd^{3+} doped potassium niobium silicate glass has exhibited relatively higher value of dielectric constant ($\epsilon = 19$) than the normal glasses sodalime silicate ($\epsilon = 7-10$) [8-10] or borosilicate glasses ($\epsilon = 4.5-8$) [6-9] due to high spontaneous polarization having empty d-orbital ($4d^0$) electronic configuration and high ionic refraction of Nb^{5+} ion ($R_i = 24.5$) as described earlier (see section 3.1). Fig. 6 shows the magnitude of dielectric constant increase steeply (from $\epsilon = 19$ to $\epsilon = 33$) in case of the heat-treated samples and thereafter it maintains saturation for any further heat treatment time. This suggests that on heat-treatment, at the initial stages, separation of silica rich phase and K–Nb enriched phases takes place and with the further prolonged heat-treatments incipient precipitation of KNbO_3 having high dielectric constant ($\epsilon = 137$) [26] and spontaneous polarization, $P_s = 0.41 \text{ C/m}^2$ [1] occurs. Thus accumulation of K^+ ions in the phase-separated glass matrix initially could cause a significant increase of dielectric constant and with further heat-treatment time, the heavy Nb^{5+} ion entering into the residual glass matrix in order to maintain the required crystallite composition, which tends to maintain a saturated value of dielectric constant. The variation in crystallite size distributions and also the distribution of the KNbO_3 phase in the microstructure are the causes for the differences in the dielectric constant values amongst the heat-treated samples [5]. This result is again in conformity with the observations made from XRD, FESEM, TEM and FTIRRS measurements on the nano-crystallization of KNbO_3 phase in the glass matrix.

3.6 Optical absorption spectra

Fig. 7 shows the representative UV-VIS-NIR absorption spectra of Nd³⁺ doped as-prepared glass (A) and heat-treated samples for 1 (B), 3 (D) and 100 h (I) duration. The spectra reveal thirteen absorption peaks due to the $4f-4f$ forced electric dipole transitions from the ground $^4I_{9/2}$ state to different excited states of Nd³⁺ ion in $4f^3$ configuration. The absorption peaks are found to be similar to those appeared in alumino silicate and chloro sulphide glasses [13, 14, 27-29]. All the peaks $^4I_{9/2} \rightarrow ^2P_{1/2}+^2D_{5/2}$ (430 nm), $^2G_{9/2}+^4G_{11/2}+^2K_{15/2}+^2D_{3/2}$ (473.6 nm), $^4G_{9/2}+^2K_{13/2}$ (513.8 nm), $^4G_{7/2}$ (529.7 nm), $^2G_{7/2}$ (574.4 nm), $^4G_{5/2}$ (584.9 nm), $^2H_{11/2}$ (625.3 nm), $^4F_{9/2}$ (683.6 nm), $^4F_{7/2}$ (741 nm), $^4S_{3/2}$ (749.4 nm), $^2H_{9/2}$ (799.4 nm), $^4F_{5/2}$ (807.9 nm) and $^4F_{3/2}$ (881 nm) are assigned in accordance with Carnall's convention [30]. From this figure it is noticed that the base line of absorption spectrum of heat-treated sample for 100 h (curve I) has been elevated significantly with the diminishing intensities of the absorption peaks. This phenomenon confirms that the laser active Nd³⁺ ions entering into the crystalline phase similar to the observation made earlier in Eu³⁺ doped KNbO₃ glass-ceramics [31].

The uplifting of the base line for glass-ceramic samples is due to scattering imparted by the nanocrystallite phase discussed as follows. Normally the decrease of optical transmission of the glass-ceramics happen mainly because of two reasons, one is crystalloid size and the other refractive index difference between crystalline and residual amorphous phase. In this system, the crystallite size observed to be in nanometric scale, and smaller than the visible wavelength. But the refractive index of the formed KNbO₃ phase (RI = 2.2912 at 600 nm) [32] is considerably higher than the residual glassy phase (RI = 1.761098 at 643.8 nm, see Table 1); hence the later case may be responsible for

changes observed in the measured optical absorption spectra. This is in accordance to the Rayleigh scattering model since the crystallites (7-11 nm) are smaller than $\lambda/20$ for visible wavelengths. The scattering loss τ , is given by [33]

$$\tau = 32\pi^4 d^3 (n\Delta n)^2 NV / 3\lambda^4 \quad (2)$$

where d is the crystallite diameter, λ the wavelength of light, n the refractive index, N the number density of crystallites, and V the volume of the crystallite. From the absorption spectra (Fig. 7) it is seen that scattering loss in the lower wavelength side is more than in the higher wavelength side. From XRD and FESEM it is observed that the crystallite diameter, their number density and volume increase with heat-treatment time. Hence the scattering loss is supported by the Eq. (2), where the refractive index of the formed crystal phase is more than the residual glass phase.

Among all the recorded absorption peaks, ${}^4I_{9/2} \rightarrow {}^4G_{5/2}, {}^2G_{7/2}$ is more intense over the others. This transition happens to be hypersensitive transition in $4f^3$ configuration obeying the selection rules $\Delta J \leq 2$, $\Delta L \leq 2$ and $\Delta S = 0$ with large value (0.898) of squared reduced matrix element, $|U^{(2)}|^2$. It is well known that in rare earth ions, these hypersensitive transitions exhibit substantial sensitivity in their band energies (positions), oscillator strengths and shapes even to minor variations in the immediate coordination environment around the ion. Their sensitivity is attributed to the changes in local symmetry and RE³⁺-O bond covalency. For the case of Nd³⁺, in addition to the hypersensitive ${}^4I_{9/2} \rightarrow ({}^4G_{5/2}, {}^2G_{7/2})$ transition, other transition such as ${}^4I_{9/2} \rightarrow ({}^4F_{7/2}, {}^4S_{3/2})$ has been considered as pseudohypersensitive transition although it does not follow strictly the selection rule but still reflects its sensitivity to the environment changes.

In the present investigation, we adopt these two absorption transitions to systematically understand the changes that are occurring in the vicinity of the dopant ions during the bulk nanocrystallization of KNbO_3 in the glass matrix. From Fig. 7, it is noticed that there is no appreciable shift in the absorption band peak positions of the hypersensitive transitions with increase in heat-treatment duration. But on careful observation, it is clear that there is a variation in their spectral profile. In absorption spectrum of sample A, the hypersensitive transition ${}^4\text{I}_{9/2} \rightarrow {}^4\text{G}_{5/2}, {}^2\text{G}_{7/2}$ is not resolved fully. It is due to the varied Nd^{3+} sites which do exist normally in glass matrix leading to the inhomogeneous broadening. But in the samples B, D and I, this peak gets resolved into two well defined peaks whose relative intensities are continuously changing with the heat treatment duration. The relative intensity ratios, of the long (I_L) to short (I_S) stark components of the transitions ${}^4\text{I}_{9/2} \rightarrow ({}^4\text{G}_{5/2}, {}^2\text{G}_{7/2})$ and ${}^4\text{I}_{9/2} \rightarrow ({}^4\text{F}_{7/2}, {}^4\text{S}_{3/2})$, have been calculated and listed in Table 2. It is known that the increase in the intensity ratio (I_L/I_S) indicates the shift of barycenter of the absorption peak to longer wavelength implying increase in covalency of RE-ligand bond. From the data presented in Table 2 it is seen that the intensity ratio values are decreasing from glass to heat treated samples denoting a very slight decrease in rare earth – ligand bond covalency. The possible explanation may be given as follows. When the precursor glass is heat treated, initially it is under going phase separation of silica rich and K-Nb rich phases followed by bulk crystallisation of KNbO_3 nano-crystallites. It is supposed that Nd^{3+} ions occupy substitutional sites of K^+ in KNbO_3 . Here, the presence of highly polarisable Nb^{5+} ions may cause the decrease in Nd-O covalency. Hence absorption peak intensity ratio changes reflect the entering of Nd^{3+} ions into the nano KNbO_3 crystallites in the glass ceramic samples.

3.7 Emission, excitation and lifetime

The emission spectra of samples A, B, D and I excited at 817 nm are depicted in Fig. 8(a). Fig. 8(b) shows their excitation spectra measured in the wavelength range 350–950 nm by monitoring with the intense NIR emission band located at 1068 nm. The spectra in Fig. 8(a) of sample-A (glass) demonstrated emissions from ${}^4F_{3/2}$ excited level to the lower levels ${}^4I_{9/2}$, ${}^4I_{11/2}$ and ${}^4I_{13/2}$ peaking at 897, 1068 and 1342 nm respectively with no observable Stark splitting. It can be seen that the most intense emission band is located at 1068 nm for the as-prepared glass and heat-treated samples. It is generally observed that the glass-ceramics samples show more intense photoluminescence compared to as-prepared glass when RE ions readily partitioned into the crystal phase [33]. Here the fluorescence intensity first decreases for the glass-ceramics heat-treated for shortest duration (1h) and then increases but with low intense than as-prepared glass. This may be due to the fact that in the short durations of heat-treatment the samples are phase separated and stable KNbO_3 phase grows with longer heat-treatment. This is also supported by the dielectric data and absorption spectra. These changes in emission spectra of glass-ceramics could establish the fact that initially the rare earth ions enter in a less amount into the crystalline phase thus formed. The Nd^{3+} ions have partitioned into the residual glassy phase and thereby caused fluorescence quenching due to concentration quenching as described in details later. The mechanism of fluorescence emission and concentration quenching due to cross relaxation (CR) and energy migration (EM) are depicted in Fig. 9. Campbell and Suratwala [34] have suggested a similar mechanism for concentration quenching in Nd-doped high power phosphate laser glasses. Kang, *et. al* [35] have also observed a similar less intense fluorescence in glass-ceramics than the as

prepared glass of neodymium activated lithium aluminosilicate system. In the perovskite type RNbO_3 ($\text{R} = \text{Li, Na, K}$) crystals, R^+ and Nb^{5+} occupy octahedral sites with C_3 or nearly C_{3v} point symmetry. When the rare earth ion is entering in the crystal, it prefers to replace R^+ site forming $[\text{REO}_6]^{9-}$ octahedron [36-38]. In the present system also, the Nd^{3+} ions replace K^+ ion sites in the formed KNbO_3 crystallites due to the closeness of their ionic radii ($\text{Nd}^{3+} = 1.12 \text{ \AA}$ and $\text{K}^+ = 1.38 \text{ \AA}$). However, still there exists slight difference in the ionic radius between the dopant (Nd^{3+}) and the host ions (K^+) along with the excess electronic charge on the dopant. Generally, when the impurity ion carries extra charge than the replaced host ion, the electrostatic force acting on the impurity is greater than that on the host ion, the impurity ion will pull the oxygen ligands inwards along impurity–ligand bonds, creating distortion in the lattice structure and as a result, distorted $[\text{NdO}_6]^{9-}$ octahedron is formed with Nd^{3+} ion facing an off-center displacement from C_3 axis in the oxygen octahedron [39, 40]. All these results are in accordance with XRD, FESEM, TEM and FTIRRS results.

Fig. 10 presents representative curves of the room temperature fluorescence decay curves of the emission transition (${}^4\text{F}_{3/2} \rightarrow {}^4\text{I}_{11/2}$) at 1068 nm with an excitation at 817 nm for Nd^{3+} ions in as-prepared glass and heat-treated samples for 1, 3 and 100 h. All the curves demonstrate a single exponential decay. The fluorescence lifetimes (τ_f) for all the samples have been estimated from these decay curves and the results of 0, 1, 3 and 100 h duration are shown in Table 2. These data indicate a decrease in the lifetime at the start of the heat-treatment and then an increasing trend with an increase of the heat-treatment duration following the similar trend as emission characteristics. It is clear that the excited state lifetime of Nd^{3+} ions initially has decreased from 269 μs for precursor glass down to

250 μs for 1 h heat-treated sample and then noticeably increases up to 298 μs for 100 h heat-treatment. The decrease in the lifetime first and then subsequent increase for further increase in heat-treatment duration may be attributed to the possible occurrence of surface defects and/or clustering of Nd^{3+} ions which act as luminescence quenchers. This may also be the reason for the observed reduction in the luminescence intensity of heat-treated glass-ceramics when compared to the as-prepared glass (see Fig. 8(a)). Dejneka [33] have demonstrated in fluoride glasses that clustering thereby quenching occur when the Eu^{3+} - Eu^{3+} ionic separation is less than 40 Å. In the present case, the Nd^{3+} - Nd^{3+} ionic separation (R_i) in the precursor glass is found to be about 26 Å which was calculated using the relation [41]:

$$R_i (\text{Å}) = (1/N_{\text{Nd}^{3+}})^{1/3} \quad (3)$$

where $N_{\text{Nd}^{3+}}$ is the Nd^{3+} ion concentration as already provided in Table 1. It is, therefore, seen that the Nd^{3+} - Nd^{3+} ionic separation (R_i) is in the quenching region. Theoretically, the rate of relaxation due to concentration quenching varies as R_i^{-6} [34, 41]. In the initial stages of heat-treatment with the formation of KNbO_3 crystal phase, the Nd^{3+} ions partitioned into the residual glassy phase by reducing the inter-ionic separation less than 26 Å of precursor glasses. This fact results in reduction in fluorescence intensity (see curve-B, Fig. 8) and lifetime (Table 2) due to concentration quenching. Later with the increase of heat-treatment time, the Nd^{3+} ions become well organized and finely dispersed in the crystal phase, thereby increasing the intensity of fluorescence and lifetime. The mechanism of concentration quenching of Nd^{3+} is already depicted in Fig. 9. Subsequent increase in lifetime is due to partitioning of Nd^{3+} ions into low phonon energy ($\sim 749 \text{ cm}^{-1}$) KNbO_3 crystal from high phonon energy ($\sim 1100 \text{ cm}^{-1}$) mother silicate

glass matrix. This process results in reduction in nonradiative decay rate due to multiphonon relaxation thereby rising in radiative decay rate. Thus, the measured fluorescence lifetime (τ_f) may be well explained by the following expression [17]:

$$\tau_f = 1/(A_{\text{rad}} + W_{\text{nr}}) \quad (4)$$

where A_{rad} and W_{nr} are the probabilities for radiative and nonradiative processes respectively. The W_{nr} includes relaxation by multiphonon emission and effective energy transfer rates arising from Nd^{3+} - Nd^{3+} ion interactions, that is, cross relaxation (CR) and energy migration (EM) as shown in Fig. 9.

In this system, with low dopant (Nd^{3+}) concentration the energy transfer may be explained by considering dipole-dipole interactions only. According to this the energy transfer interactions strongly depend on the concentration of donor (Nd^{3+}) and acceptor (Nd^{3+}) ions. It has also been shown that diffusion to play a minor role in energy transfer at low dopant concentrations [42]. In the case of very fast diffusion, the fluorescence decay curve is purely exponential and the quenching rate shows a linear dependence on concentration [43]. Here with heat-treatment time as the Nd^{3+} concentration in the crystal phase increases the rate of energy transfer also increases. The energy transfer in our case is a cross relaxation (CR) through fast diffusion process. Consequently, it can be expected that the Yokota-Tanimoto model [44] is valid for low Nd^{3+} concentrations in the glass system.

4. Conclusions

Nd_2O_3 (0.5 wt%) doped nanometric KNbO_3 crystallites containing glass-ceramics were prepared from the glass $25\text{K}_2\text{O}$ - $25\text{Nb}_2\text{O}_5$ - 50SiO_2 (mol%) by an isothermal

crystallization at 800°C for different durations. The formation of nano-crystallite of KNbO₃ in the glass matrix was confirmed by the XRD, FESEM, TEM, FTIRRS and dielectric constant measurements. The crystallite size estimated from XRD and TEM is found to vary in the range of 7-11 nm. The optical absorption spectra, decay time fluorescence spectra of heat-treated glass-ceramic samples demonstrate that the Nd³⁺ ion has gradually entered into the KNbO₃ crystalline phase with increase in heat-treatment time.

Acknowledgements

This research work was supported by BRNS/DAE under the sanction No. 2007/34/05-BRNS. They gratefully thank Dr. H. S. Maiti, Director of the institute for his keen interest and kind permission to publish this paper. The technical supports provided by the infrastructural facility (X-ray and Electron Microscopy Divisions) of this institute are also thankfully acknowledged.

References

- [1] W. P. Risk, T. R. Gosnell, A. V. Nurmikko, *Compact Blue-Green Lasers*, Cambridge University Press, Cambridge, 2003.
- [2] M. Zgonik, R. Schlessler, I. Biaggio, E. Voit, J. Tscherry, P. Giinter, *J. Appl. Phys.* 74 (1993) 1287.
- [3] D. F. Xue, S. Y. Zhang, *Chem. Phys. Lett.* 291 (1998) 401.
- [4] E. Ringgaard, T. Wurlitzer, *J. Eur. Ceram. Soc.* 25 (2005) 2701.
- [5] D. E. Vernacotola, *Key Engg. Mater.* 94-95 (1994) 379.
- [6] P. Pernice, A. Aronne, V. N. Sigaev, P. D. Sarkisov, V. I. Molev, S. Y. Stefanovich, *J. Am. Ceram. Soc.* 82 (1999) 3447.
- [7] P. Pernice, A. Aronne, V. N. Sigaev, M. Kupriyanova, *J. Non-Cryst. Solids* 275 (2000) 216.
- [8] V. V. Golubkov, O. S. Dymshits, A. A. Zhilin, A. V. Redin, M. P. Shepilov, *Glass Phys. Chem.* 27 (2001) 504.
- [9] H. Tanaka, M. Yamamoto, Y. Takahashi, Y. Benino, T. Fujiwara, T. Komatsu, *Opt. Mater.* 22 (2003) 71.
- [10] A. Aronne, V. N. Sigaev, P. Pernice, E. Fanelli, L. Z. Usmanova, *J. Non-Cryst. Solids* 337 (2004) 121.
- [11] P. Zeller, P. Peuser, *Opt. Lett.* 25 (2000) 34.
- [12] F. Lahoz, I. R. Martín, U. R. Roríguez-Mendoza, I. Iparraguirre, J. azkargorta, A. Mendioroz, R. Balda, J. fernández and V. Lavín, *Opt. Mater.* 27 (2005) 1762.
- [13] M. C. Silva, F. H. Cristovan, C. M. Nascimento, M. J. V. Bell, W. O. Cruz, A. Marletta, *J. Non-Cryst. Solids* 352 (2006) 5296.

- [14] V. Seznec, H. L. Ma, X. H. Zhang, V. Nazabal, J-L. Adam, X. S. Qiao, X. P. Fan, *Opt. Mater.* 29 (2006) 371.
- [15] S. Mohan, K. S. Thind, G. Sharma, L. Gerward, *Spectrochim. Acta A* 70 (2008) 1173.
- [16] M. B. Volf, *Chemical Approach to Glass*, Elsevier, Amsterdam, 1984.
- [17] M. Yamane, Y. Asahara, *Glasses for Photonics*, Cambridge University Press, Cambridge, UK, 2000.
- [18] D. E. Vernacotola, J. E. Shelby, *Phys. Chem. Glasses* 35 (1994) 153.
- [19] D. E. Vernacotola, J. E. Shelby, *Ceram. Trans.* 29 (1993) 215.
- [20] B. D. Cullity, *Elements of X-Ray Diffraction*, 2nd ed. Addison-Wesley Publishing Co., London, UK, 1977.
- [21] A. Aronne, V. N. Sigaev, B. Champagnon, E. Fanelli, V. Califano, L. Z. Usmanova, P. Pernice, *J. Non-Cryst. Solids* 351 (2005) 3610.
- [22] K. Fukumi, S. Sakka, *J. Mater. Sci.*, 23 (1988) 2819.
- [23] B. Sumuneva, St. Kralchev, V. Dimitrov, *J. Non-Cryst. Solids*, 129 (1991) 54.
- [24] J. S. deAndrade, A. G. Pinheiro, I. F. Vasconcelos, M. A. B. deArujo, M. A. Valente, A. S. B. Sombra, *J. Phys. Chem. Solids* 61 (2000) 899.
- [25] E. N. Silva, A. P. Ayala, I. Guedes, C. W. A. Paschoal, R. L. Moreira, C. K. Loong, L. A. Boatner, *Opt. Mater.* 29 (2006) 224.
- [26] A. Z. Simões, A. Ries, C. S. Riccardi, A. H. Gonzalez, M. A. Zaghete, B. D. Stojanovic, M. Cilense, J. A. Varela, *Mat. Lett.* 58 (2004) 2537.
- [27] S. Hazarika, S. Rai, *Opt. Mater.* 30 (2007) 462.
- [28] T. Ishizaka, Y. Kurokawa, T. Makino, Y. Segawa, *Opt. Mater.* 15 (2001) 293.

- [29] B. Frumarová, M. Frumar, J. Oswald, *J. Non-Cryst. Solids* 213 & 214 (1997) 58.
- [30] W. T. Carnall, P. R. Fields, K. Rajnak, *J. Chem. Phys.* 49 (1968) 4424.
- [31] R. S. Chaliha, K. Annapurna, A. Tarafder, V. S. Tiwari, P. K. Gupta, B. Karmakar, *Solid State Sci.* 11 (2009) 1325.
- [32] E. D. Palik, *Handbook of Optical Constants of Solids III*, Academic Press, San Diego, 1998, p. 834.
- [33] M. J. Dejneka, *J. Non-Cryst. Solids* 239 (1998) 149.
- [34] J. H. Campbell, T. I. Suratwala, *J. Non-Cryst. Solids* 263 & 264 (2000) 318.
- [35] U. K. Kang, A. A. Zhilin, D. P. Logvinov, A. A. Onushchenko, V. A. Savost'yanov, T. I. Chuvaeva, A.V. Shashkin, *Glass Phys. Chem.* 27 (2001) 344.
- [36] S. Y. Wu, W. C. Zheng, *Phys. Rev. B* 65 (2002) 224107.
- [37] S. Y. Wu, H. N. Dong, *J. Alloy. Comp.* 386 (2005) 52.
- [38] Y. M. Chang, T. H. Yeom, Y. Y. Yeung, C. Rudowicz, *J. Phys. C : Conds. Mater.* 5 (1993) 6221.
- [39] D. M. B. P. Milori, I. J. Moraes, A. C. Hernandez, R. R. de Souza, M. Siu Li, M. C. Terrile, G. E. Barberis, *Phys. Rev. B* 51 (1995) 3206.
- [40] Z. C. -Xia, K. Xiao -Yu, M. A. Jie, W. Hui, *Phys. B* 403 (2008) 3114.
- [41] K. Pátek, *Glass Lasers*, Butterworth & Co (Publishers) Ltd., London, 1970.
- [42] K. K. Mahato, D. K. Rai, S. B. Rai, *Phys. Stat. Sol. (a)* 174 (1999) 277.
- [43] R. Balda, J. Fernández, S. García-Revilla, J. M. Fernández-Navarro, *Opt. Exp.* 15 (2007) 6750.
- [44] M. Yokota, O. Tanimoto, *J. Phys. Soc. Jpn.* 22 (1967) 779.

Figure Captions

Fig. 1. DTA curve of as-prepared precursor glass powder.

Fig. 2. (Color online) Photograph showing the transparency, as laid on writing, of the (a) as-prepared glass and heat-treated samples at 800°C for (b) 1, (c) 2, (d) 3, (e) 5, (f) 10, (g) 25, (h) 50 and (i) 100 h.

Fig. 3. (a) XRD patterns of (A) as-prepared glass and heat-treated glasses at 800°C for (B) 1, (C) 2, (D) 3, (E) 5, (F) 10, (G) 25, (H) 50 and (I) 100 h. (b) Variation of crystallite size, as obtained from XRD, as a function of heat-treatment time at 800°C of as-prepared glasses.

Fig. 4. FESEM photomicrograph of heat-treated glasses at 800°C for (a) 5 and (b) 100 h (scale bar = 100 nm). TEM image of 100 h heat-treated sample (c) bright field image (inset : SAED), and (d) HRTEM image of lattice fringe.

Fig. 5. Comparative FTIR spectra of the (A) as-prepared glass and heat-treated glasses at 800°C for (B) 1 and (I) 100 h. Inset shows FTIR spectra of the (A) as-prepared glass, (B) 1, (C) 2, (D) 3, (E) 5, (F) 10, (G) 25, (H) 50 and (I) 100 h.

Fig. 6. Dielectric constant of as-prepared glass and glass-ceramics as a function of heat-treatment time at 800°C.

Fig. 7. Absorption spectra of the (A) as-prepared glass and heat-treated glasses at 800°C for (B) 1, (D) 3 and (I) 100 h (Transitions are from the ground state $^4I_{9/2}$).

Fig. 8. (a) Emission spectra ($\lambda_{\text{ex}} = 817$ nm) of the (A) as-prepared glass and heat-treated glasses at 800°C for (B) 1, (D) 3 and (I) 100 h. (b) Their excitation spectra ($\lambda_{\text{em}} = 1068$ nm).

Fig. 9. Partial energy level diagram of Nd^{3+} in the present glass system showing excitation at 817 nm and emission at 897, 1068 and 1342 nm (Here, GSA = Ground state absorption, CR = Cross relaxation, EM = Energy migration, NR = Non-radiative transition and R = Radiative transition).

Fig. 10. Decay curves for the $^4F_{3/2} \rightarrow ^4I_{11/2}$ transition at 1068 nm under excitation at 817 nm of (A) as-prepared glass and heat-treated glasses at 800°C for (B) 1, (D) 3 and (I) 100 h.

Table 1

Some measured and calculated properties of 25K₂O-25Nb₂O₅-50SiO₂ (mol %) glass with 0.5 wt% Nd₂O₃ (in excess)

| Properties | Corresponding value |
|--|-------------------------|
| Average molecular weight | 120.05 |
| Density, g.cm ⁻³ | 3.16 |
| Refractive index | |
| n _e (at 546.1 nm) | 1.774764 |
| n _{F'} (at 480.0 nm) | 1.787999 |
| n _{C'} (at 643.8 nm) | 1.761098 |
| Mean dispersion (n _{F'} - n _{C'}) | 0.026901 |
| Abbe number, n _e /(n _{F'} -n _{C'}) | 29 |
| Reflection loss (%) | 7.80 |
| Molar refractivity, R _M (cm ³) | 15.86 |
| Electronic polarizability, α (cm ³) | 6.286×10 ⁻²⁴ |
| Nd ³⁺ ion concentration, N _{Nd³⁺} (ions/cm ³) | 5.71×10 ¹⁹ |
| Nd ³⁺ -Nd ³⁺ inter ionic distance, R _i (Å) | 26 |
| Glass transition temperature, T _g (°C) | 669 |
| First crystallization peak, T _{p1} (°C) | 760 |
| Second crystallization peak, T _{p2} (°C) | 935 |

Table 2

Relative intensity ratio of I_{Nb-O}/I_{Si-O} from FTIRR spectra and stark components ⁴G_{5/2}/²G_{7/2} and ⁴S_{3/2}/⁴F_{7/2} from absorption spectra and measured lifetime (τ_f) of the ⁴F_{3/2} → ⁴I_{11/2} emission transition of precursor and heat treated Nd³⁺ doped glasses at 800°C

| Sample identity | Heat treatment time (h) | Relative intensity ratio | | | Lifetime, τ _f (μs) |
|-----------------|-------------------------|---|-------------------------------------|-------------------------------------|-------------------------------|
| | | FTIR I _{Nb-O} / I _{Si-O} | Absorption | | |
| | | | $\frac{I(^4G_{5/2})}{I(^2G_{7/2})}$ | $\frac{I(^4S_{3/2})}{I(^4F_{7/2})}$ | |
| A | 0 | - | 1.37 | 1.02 | 269 |
| B | 1 | 1.09 | 1.21 | 0.91 | 250 |
| D | 3 | 1.11 | 1.19 | 0.91 | 276 |
| I | 100 | 1.12 | 1.15 | 0.89 | 298 |

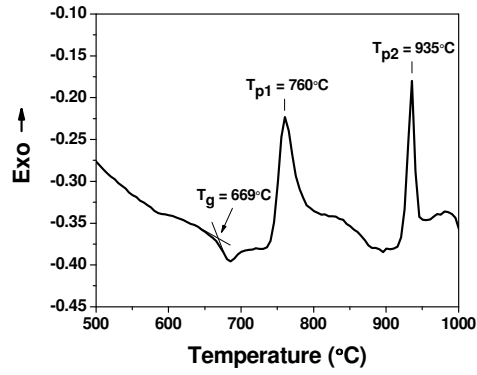


Fig. 1. DTA curve of as-prepared precursor glass powder.



Fig. 2. (Color online) Photograph showing the transparency, as laid on writing, of the (a) as-prepared glass and heat-treated samples at 800°C for (b) 1, (c) 2, (d) 3, (e) 5, (f) 10, (g) 25, (h) 50 and (i) 100 h.

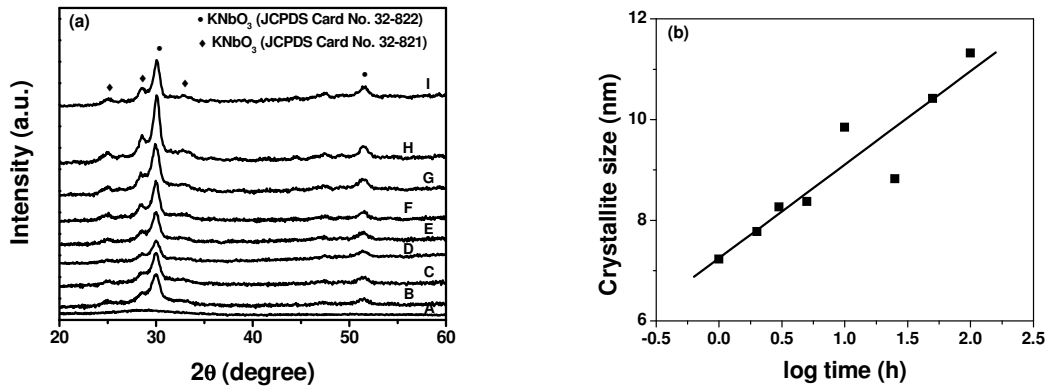


Fig. 3. (a) XRD patterns of (A) as-prepared glass and heat-treated glasses at 800°C for (B) 1, (C) 2, (D) 3, (E) 5, (F) 10, (G) 25, (H) 50 and (I) 100 h. (b) Variation of crystallite size, as obtained from XRD, as a function of heat-treatment time at 800°C of as-prepared glasses.

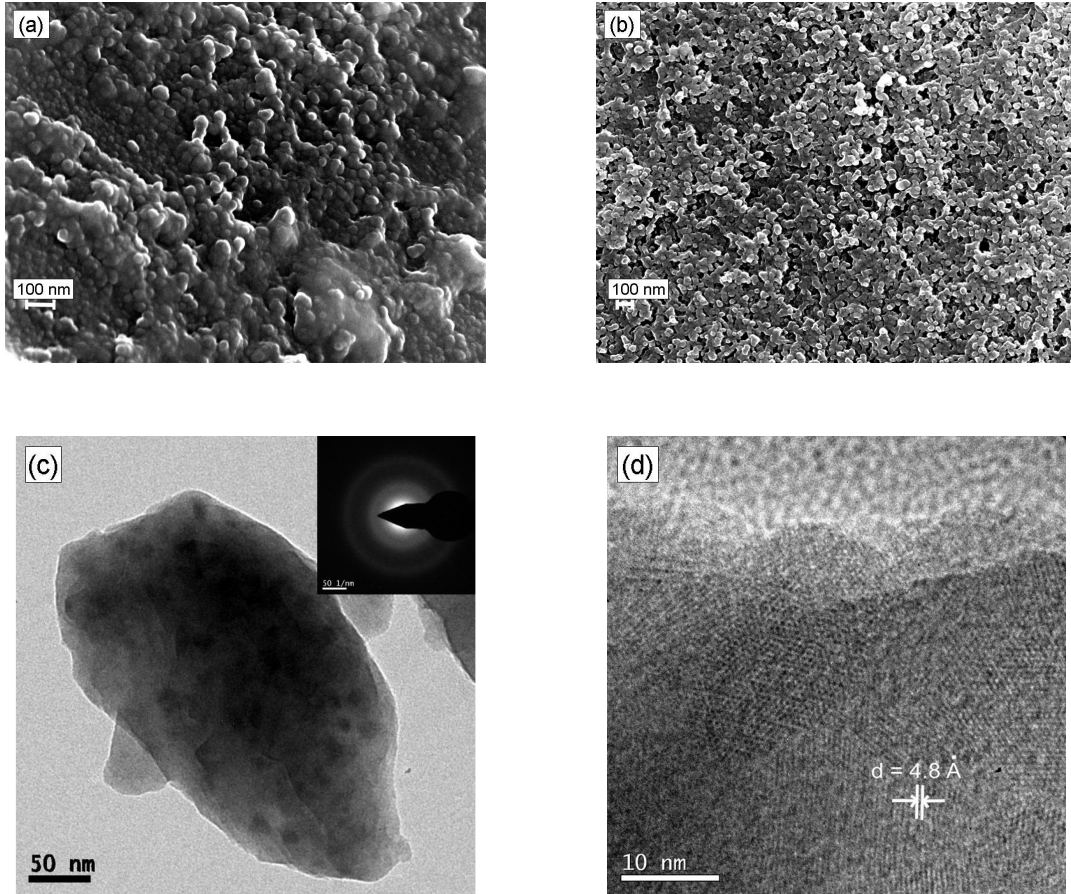


Fig. 4. FESEM photomicrograph of heat-treated glasses at 800°C for (a) 5 and (b) 100 h (scale bar = 100 nm). TEM image of 100 h heat-treated sample (c) bright field image (inset : SAED), and (d) HRTEM image of lattice fringe.

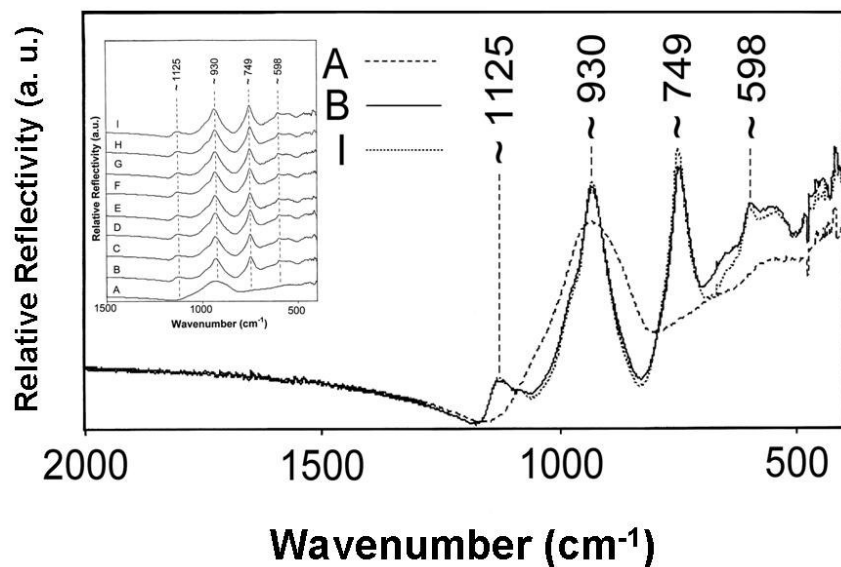


Fig. 5. Comparative FTIR spectra of the (A) as-prepared glass and heat-treated glasses at 800°C for (B) 1 and (I) 100 h. Inset shows FTIR spectra of the (A) as-prepared glass, (B) 1, (C) 2, (D) 3, (E) 5, (F) 10, (G) 25, (H) 50 and (I) 100 h.

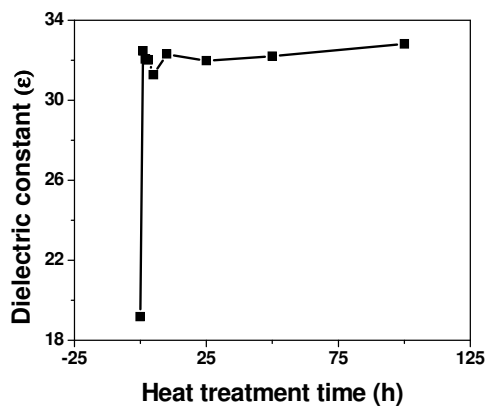


Fig. 6. Dielectric constant of as-prepared glass and glass-ceramics as a function of heat-treatment time at 800°C.

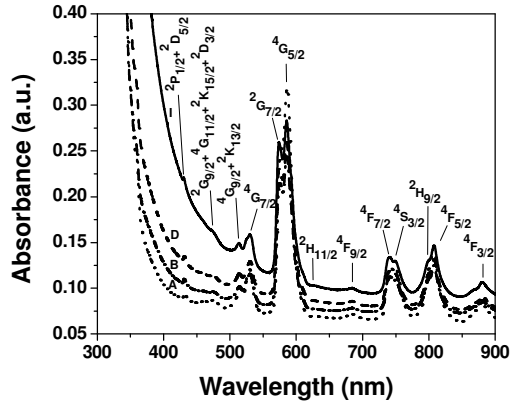


Fig. 7. Absorption spectra of the (A) as-prepared glass and heat-treated glasses at 800°C for (B) 1, (D) 3 and (I) 100 h (Transitions are from the ground state $^4I_{9/2}$).

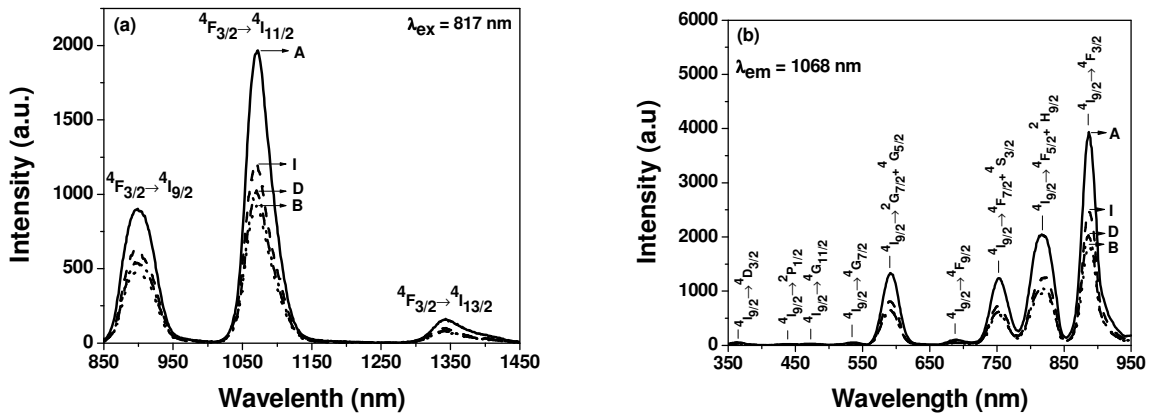


Fig. 8. (a) Emission spectra ($\lambda_{\text{ex}} = 817 \text{ nm}$) of the (A) as-prepared glass and heat-treated glasses at 800°C for (B) 1, (D) 3 and (I) 100 h. (b) Their excitation spectra ($\lambda_{\text{em}} = 1068 \text{ nm}$).

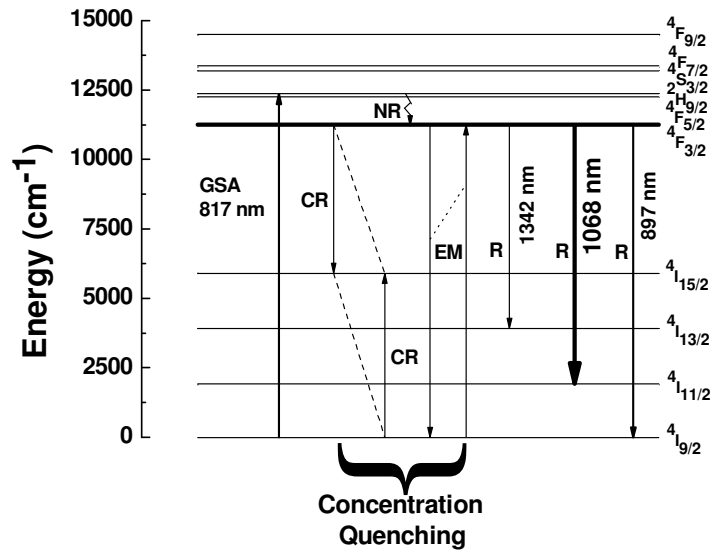


Fig. 9. Partial energy level diagram of Nd^{3+} in the present glass system showing excitation at 817 nm and emission at 897, 1068 and 1342 nm (Here, GSA = Ground state absorption, CR = Cross relaxation, EM = Energy migration, NR = Non-radiative transition and R = Radiative transition).

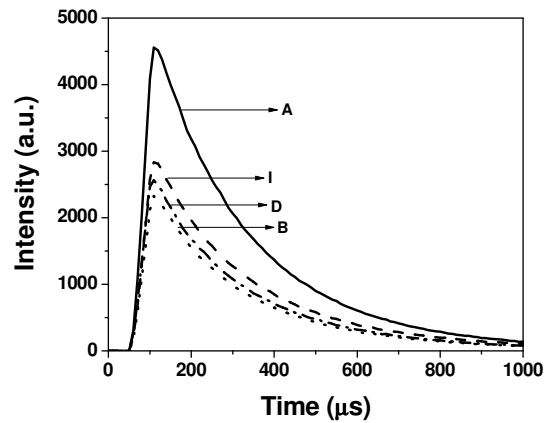


Fig. 10. Decay curves for the ${}^4\text{F}_{3/2} \rightarrow {}^4\text{I}_{11/2}$ transition at 1068 nm under excitation at 817 nm of (A) as-prepared glass and heat-treated glasses at 800°C for (B) 1, (D) 3 and (I) 100 h.